







Research Article

Independently Tunable Triband Patch Antenna with Band-Notched Characteristics for X-Band Applications

Thi Kieu Nga Le ^{1,2}, **Fabian Schwartau** ¹, **Sebastian Paul** ¹, **Duy Tung Phan** ³,
Ping Jack Soh ³ and **Joerg Schoebel** ¹

¹*Institut für Hochfrequenztechnik, Technische Universität Braunschweig, Braunschweig 38106, Germany*

²*School of Engineering and Technology, Vinh University, Vinh 460000, Vietnam*

³*Centre for Wireless Communications-Radio Technologies, University of Oulu, Oulu 90014, Finland*

Correspondence should be addressed to Thi Kieu Nga Le; ngaledhv@gmail.com

Received 15 December 2022; Revised 4 May 2023; Accepted 20 May 2023; Published 15 June 2023

Academic Editor: Flaminio Ferrara

Copyright © 2023 Thi Kieu Nga Le et al. This is an open access article distributed under the Creative Commons Attribution License, which permits unrestricted use, distribution, and reproduction in any medium, provided the original work is properly cited.

This paper presents a triband antenna with a simple design for X-band applications. The proposed antenna is designed based on a patch with a truncated corner slot and complementary split-ring resonators in the ground plane. In this way, the antenna exhibits three operating bands and its resonant frequencies can be controlled independently by changing dimensions of the slot in the patch and the resonator structures in the ground plane. In addition, due to the antiresonant behavior of the complementary split-ring resonator structures, the antenna exhibits a notch-band characteristic at 10.7 GHz. A parametric study is performed to provide a detailed understanding of the independent resonance tuning behavior of the antenna. Both simulated and measured results of the proposed antenna are presented, which are in good agreement. The proposed antenna shows three operating bands in the X-band including (with absolute and relative bandwidths) 9.4–9.7 GHz (300 MHz, 3.14%), 10.3–10.6 GHz (300 MHz, 2.86%), and 11.05–11.32 GHz (297 MHz, 2.66%). In addition to that, a notched band of 10.6–11.05 GHz is introduced to exclude operation in the frequency bands of radiometric observation systems (10.6–10.7 GHz). To the best of our knowledge, this work is unique in its combination of independent tuning of three frequency bands of operation with single-layer implementation in the X-band. Such a structure provides additional degrees of freedom to the antenna design, customizing operation in the required bands while avoiding operation in other bands.

1. Introduction

The rapid advancement of wireless communication technology has motivated the increase of system capacity and the implementation of multimode communication. Therefore, demands for mobile terminals working in several frequency bands are increasing. Space limitations on mobile terminals and limited spectrum resources make multiband antennas more advantageous compared to single-band antennas. Such a choice simultaneously reduces the required number of antennas and maximizes operation in the required frequency bands. With several advantages of the X-band over other frequency bands such as low interference from rain fading and low noise, the X-band is used for civil, military,

government radar applications and satellite, and terrestrial communications. In the field of sensing and radar, the X-band not only hosts maritime radar but also other radar and Doppler-based motion sensing systems. These systems are applied in alarm systems, bird migration detection, or radar-activated obstruction lighting system for wind turbines. The frequency allocated for these systems may differ by country (such as motion sensing in the 9.2–10.6 GHz range), thus a multiband design that can be easily and independently tuned to operate at different frequencies will be very desirable at a global scale. Several approaches in designing multiband antennas have been proposed [1–8], such as loading U-slots on the patch with an air-gap as substrate [1], using multilayered patch structure [2], introducing

arc-shaped strips and inverted L-shape stubs [3], using a truncated-corner square slot loaded with a set of split-ring resonators (SRRs) [4], introducing slits of various sizes in a patch [5], loading metalized shorting vias and etching inverted multiple U-shapes slots to obtain size reduction and multiband behavior [6], integrating complementary splitting resonators (CSSRs) on the ground plane [7], and using E-shaped fractal patches [8]. However, these approaches are difficult to integrate into one circuit board due to the additional fabrication complexity, as they may require air-gaps [1], metallic cavity [4], multilayered structures [2], and shorting vias [6]. Moreover, the resonant frequencies of these multiband antennas cannot be controlled independently, except [4]. This then limits their design flexibility and practical applications. In addition to that, the design of a multiband antenna for high-frequency bands is rarely reported so far due to the antenna in the bands normally which is small in size, causing the resonances to be very sensitive to dimensional fabrication tolerances, making the resonant frequencies hard to be controlled independently. On the other hand, narrow operating bandwidths might be required for specific applications since a broadband antenna receives and transmits unwanted signals out of the interested band. This then requires the possible integration of preselection filters to suppress out-of-band signals, which increases design complexity. For example, X-band (8–12 GHz) hosts numerous communication, radar and sensing systems such as maritime radar, amateur radio, or short-range devices such as microwave motion sensors. High-power narrow-band systems, such as radar, may cause possible electromagnetic interference to sensitive low-power systems. The bands 10.6–10.68 GHz and specifically 10.68–10.7 GHz are used for radiometric exploration and are under regulatory protection from unwanted radiation. Therefore, system designers need to ensure that emissions, which may also originate from higher-order parasitic frequency conversion in the receiver path, are not emitted from the transmitting and receiving antennas. To overcome this, many band-notched techniques have been proposed, including square-ring patches with T-shaped slits [9], microstrip open-loop resonators [10], printed open-slot antenna [11], U-shaped parasitic strips along the feed line or in the radiator patch [12–14], an Archimedean spiral slot for filtering feature was introduced in [15], and using electromagnetic band-gap (EBG) structures [16, 17], or SRR and CSRR structures [17–21]. However, the aforementioned method cannot be applied in a straightforward manner to a multiband antenna, as this will strongly impact its resonant frequency. This becomes even more challenging when these antennas are being designed for higher frequencies such as X-band due to their size compactness. Besides providing multiband operation, a unique method of integrating the CSRR (complementary split-ring resonator) structure was also demonstrated to significantly miniaturize and improve the performance of a patch antenna [22]. This paper presents a triband antenna with notched band behavior for X-band applications. The operating frequencies of the proposed antenna can be controlled independently by tuning the dimensions of the

loaded slot as well as the CSRR structures. To the best of our knowledge, there is no multiple independent frequency tuning capability for a multiband antenna reported at such a high frequency thus far. The proposed approach to designing multiband antennas with flexible frequency assignment is effective and highly desirable for wireless devices working in the X-band.

2. Antenna Design and Simulation

2.1. Antenna Configuration. The proposed antenna is designed based on a patch antenna with several modifications on the top and bottom layers to obtain multiresonant frequency as well as notched-band characteristics. As shown in Figure 1, a truncated corner square slot is added in the square radiating patch as the top layer (Figure 1(a)). The bottom layer acts as a ground plane, which is defected by two complementary split-ring resonators (CSRRs) as shown in Figure 1(c). The radiating patch and ground plane are made from copper and separated by a dielectric layer of Rogers 5880 ($\epsilon_r = 2.2$, $\tan\delta = 0.0009$), as shown in Figure 1(b). The optimized dimensions of the proposed antenna are listed in Table 1. In the next section, parametric studies will be presented to investigate the behavior of the antenna with different dimensions and locations of the slot and the CSRR structures.

3. Simulation Results

3.1. Antenna Evolution. Figure 2 illustrates step-by-step evolution of the proposed antenna from a conventional square patch with a fundamental resonance at 11.4 GHz. By introducing a truncated corner slot on the radiating patch, an additional resonance at 9.7 GHz is produced, while the original resonance shifts downwards from 11.4 GHz to 10.8 GHz. This is a result of mode splitting of the degenerate rectangular patch modes, which distributes their currents now in the direction and perpendicular to the slot's main axis (see Figures 3(a) and 3(b)). As the next step, two CSRR structures are added onto the ground plane of the slotted antenna. The slotted antenna loaded with CSRR structures produces a higher resonance at 11.3 GHz, whereas the two lower resonances are downshifted significantly. Moreover, a frequency band notch is produced, centered at around 11 GHz, as shown in Figure 2. The creation of both the band notch and the higher antenna resonance is based on the resonant and antiresonant frequency characteristics of the CSRR structure, which is explained and illustrated in the following subsection.

3.2. Effects of the Slot. A parametric study of the slot is performed in this section to investigate its effect on the antenna's resonant frequencies. Firstly, we investigate the resonant characteristic of the antenna with different orientations of the slot, as shown in Figure 4. The slot is rotated in the patch plane around z -axis with angles of 0, 45, 90, and 135°. As shown in Figure 4, the resonance of the proposed antenna is strongly influenced by the orientation of the slot. We found that the orientation of $\phi = 45^\circ$ produces the best

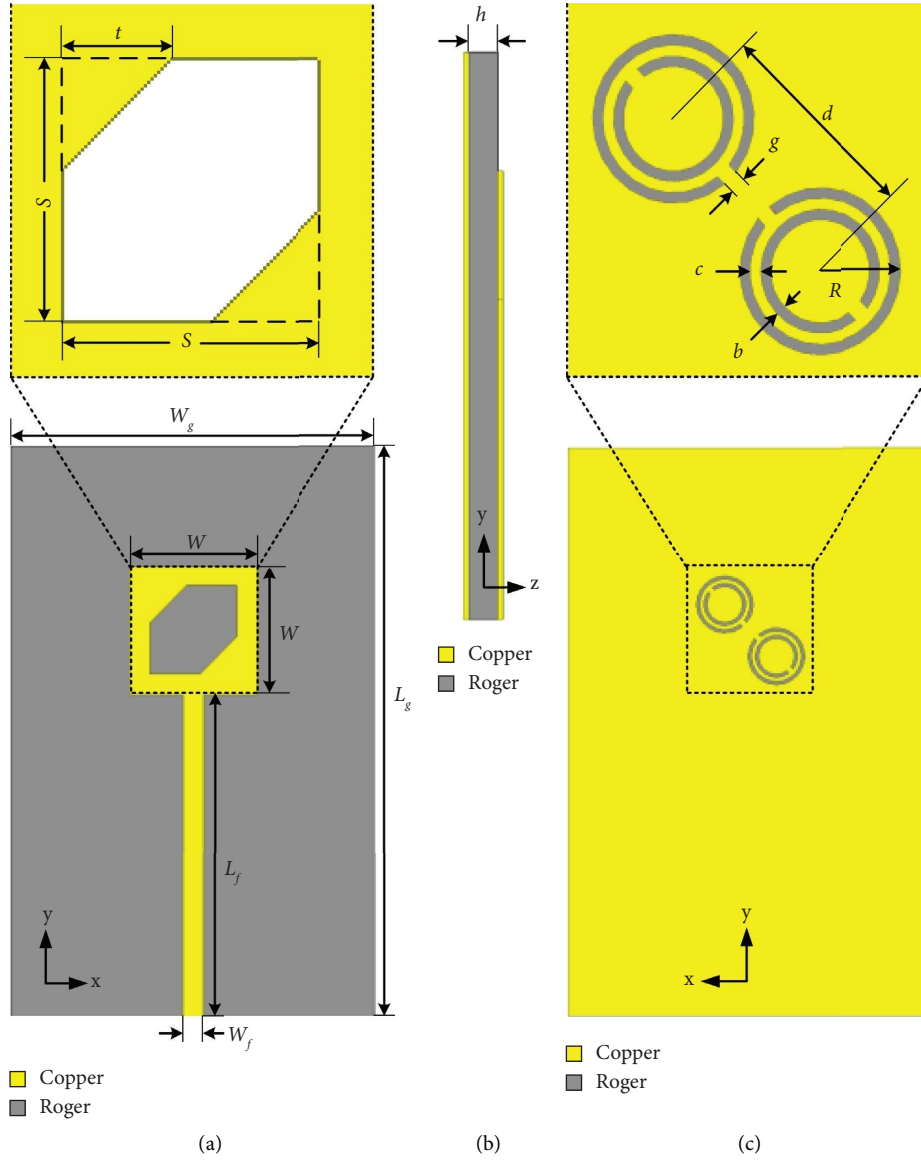


FIGURE 1: Configuration of the proposed antenna: (a) top view, (b) side view, and (c) bottom view.

TABLE 1: Dimensions of the proposed antenna.

Parameters	Values (mm)
W_g	20
W_f	1.1
W	7
S	5.2
$b = c$	0.2
R	1.56
L_g	31
L_f	17.5
d	4
t	2.4
g	0.2
h	1.57

performance in terms of number of resonances and frequency band notch. Also, the resonant behavior of the antenna versus the dimensions of the slot is then studied and

illustrated in Figure 5. As shown in Figure 5(a), when the length (S) of the slot varies from 4.9 to 5.3 mm, the lowest resonant frequency of the antenna is downshifted, while the other resonances remain almost unchanged. Similarly, Figure 5(b) illustrates that by varying the length of the truncated corners (t) from 2.3 mm to 2.6 mm, the center resonance of the antenna is shifted upwards, while both the lowest and highest resonances are nearly unaltered.

3.3. Effects of CSRR Structures. The CSRR unit cell is separately studied and its simulated scattering parameters are shown in Figure 6. In [23], the extraction of S parameters for a split-ring resonator unit cell using the perfect electric and perfect magnetic boundary condition was introduced. The inset of Figure 6 shows the simulated model of the CSRR unit cell. The boundary condition of this unit cell is constructed similar to the condition when the CSRR structures

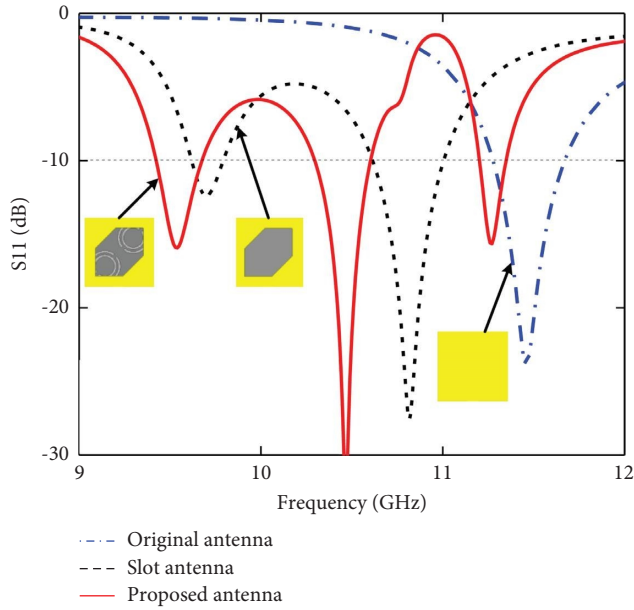


FIGURE 2: Evolution of the proposed antenna.

placed under the slot patch radiator. The perfect electric conductor (PEC) boundary condition is set up on the left and right faces of the waveguide, whereas the perfect magnetic conductor (PMC) boundary condition is set up on the front and back faces of the waveguide. Port 1 and port 2 are set up on the bottom and the top of the waveguide, respectively. The results show that the lowest values of the transmission coefficient (S_{21}) as well as the reflection coefficient (S_{11}) of the CSRR unit cell are obtained at 11 GHz and 11.3 GHz, respectively. It is evident that the designed CSRR unit cell simultaneously exhibits antiresonant behavior at 11 GHz and resonant frequency at 11.3 GHz. The characteristics of the split-ring resonator such as resonance, antiresonance, and absorption were also presented in [24, 25]. This explains the creation of the band notch at around 11 GHz and the resonance at 11.3 GHz of the proposed antenna when loaded with the CSRR structures on its ground plane.

By locating the CSRRs on the opposite side of the slotted patch, the magnetic field of the slotted patch will then excite the CSRRs. We therefore study the CSRRs' orientation to determine their best location to magnetically couple with and improve the performance of the antenna. Figure 7 shows the reflection coefficients of the antenna when the CSRRs on the ground plane are rotated around the z -axis with angles of 0, 45, 90, and 135. It is observed that the orientation of the CSRRs influences mostly the notch band and the highest resonance. When the CSRRs are placed with $\phi = 45^\circ$, the best notch-band performance at 11 GHz and the best resonant band at 11.3 GHz are achieved.

The final study in this section is carried out to understand the effect of the CSRR dimensions on the highest resonance and notch-band behavior of the antenna. The radius R of CSRR is changed from 1.55 mm to 1.58 mm, as shown in Figure 8. Both the frequency of the notch band and the highest operating frequency of the antenna can be tuned

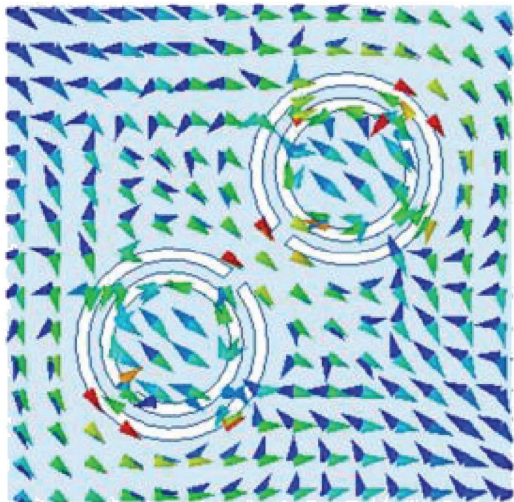
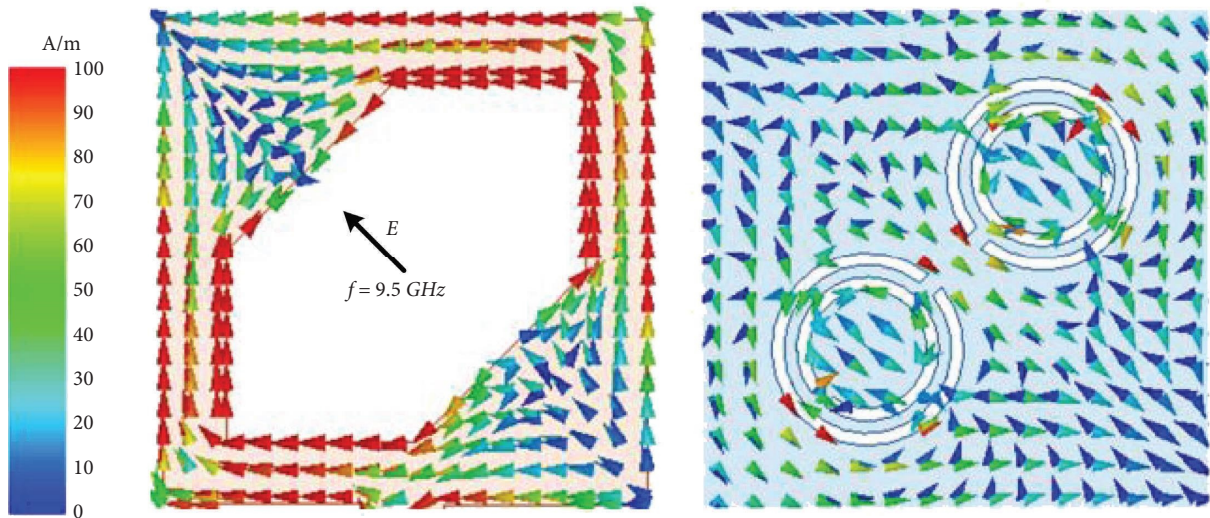
from 11.1 GHz to 10.8 GHz and from 11.41 GHz to 11.09 GHz, respectively. The lowest resonance is kept unchanged, whereas the middle resonance is slightly downshifted.

Observations from Figures 5 and 8 indicate that the resonant frequencies of the proposed antenna can be controlled independently through the varying dimensions of the slot and CSRR structures.

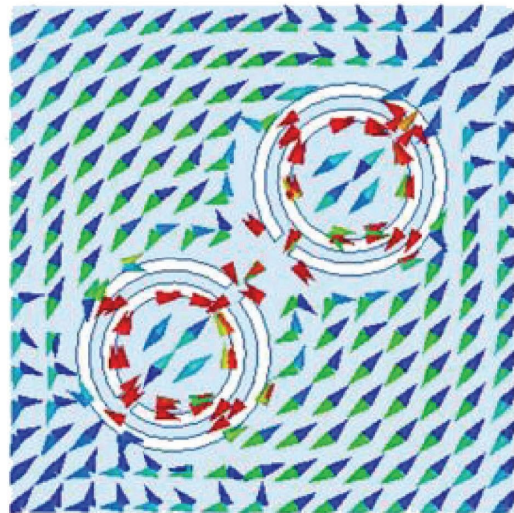
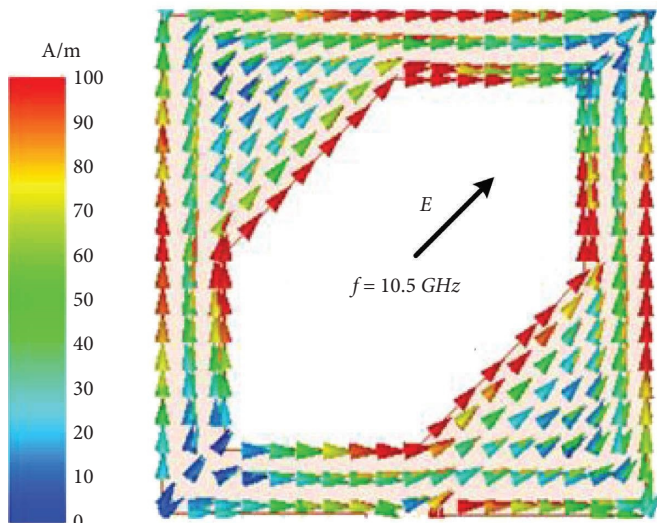
From the aforementioned parametric study, it can be concluded that (i) the best performance of the antenna in terms of operating bands and the notch band has been achieved by locating both the truncated slot and the CSRR structures at the angle of $\phi = 45^\circ$ and (ii) the resonant frequencies of the antenna can be controlled independently. The lowest resonance is tuned by varying the length of the slot (S), the middle resonance shifts upwards with the increase in length of the corner cutout (t), and the highest operating frequency is tuned by varying the CSRR radius (R).

3.4. Independent Frequency Tuning Mechanism. To better understand the physical phenomena behind the independent frequency tuning, the current distributions on the top and bottom layers of the antenna at the respective resonant and notch frequencies are simulated and presented in Figure 3. From this figure, it can be seen that the surface current at 9.5 GHz is largely distributed on the apexes (i.e., upper rightmost and lower leftmost corners) of the slot, forming a standing wave. It should be noted that the corner cutout t is fixed; therefore, the length of the current wave increases when S increases, leading to the downwards shift of this resonant frequency, as shown in Figure 5(a). At the middle resonance of 10.5 GHz, the surface current concentrates mainly on the long edges of both truncated corners of the slot (Figure 3(b)). When t is increased and S is fixed, the total length of this current wave decreases, resulting in the upward frequency shift of the middle resonance, as shown in Figure 5(b). The fixed values of t and S are listed in Table 1. At the notched frequency of 11 GHz, the surface current distribution shown in Figure 3(c) (left) is minimal on the patch, whereas the surface currents on the two CSRRs' flow in opposite directions (Figure 3(c) (right)) resulting in the mutual elimination of their electromagnetic radiation. This explains the absence of radiation from the patch antenna and the creation of the notch band.

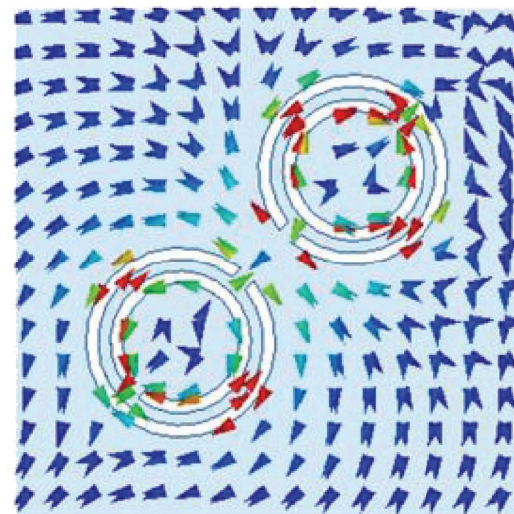
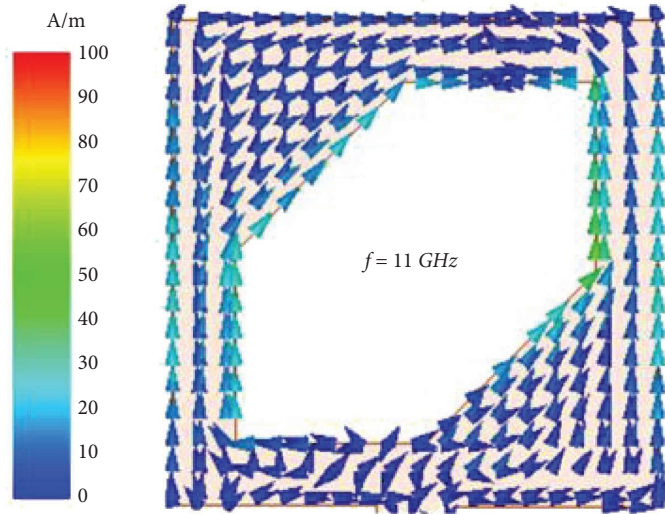
In contrast, at the highest resonance, strong equidirectional surface currents are distributed on the CSRR structures on the bottom layer (Figure 3(d) (right)). In contrast, the surface current distribution on the top layer (Figure 3(d) (left)) is significantly weaker than that observed at 9.5 and 10.5 GHz. This observation indicates that the CSRR structures are important contributors to the highest resonance at 11.3 GHz. Consequently, this resonance as well as the notch band move downwards when the radius R of the CSRR structures increases, as shown in Figure 8. At the same time, all three resonances are reasonably well decoupled, which enables their independent tuning.



(a)



(b)



(c)

FIGURE 3: Continued.

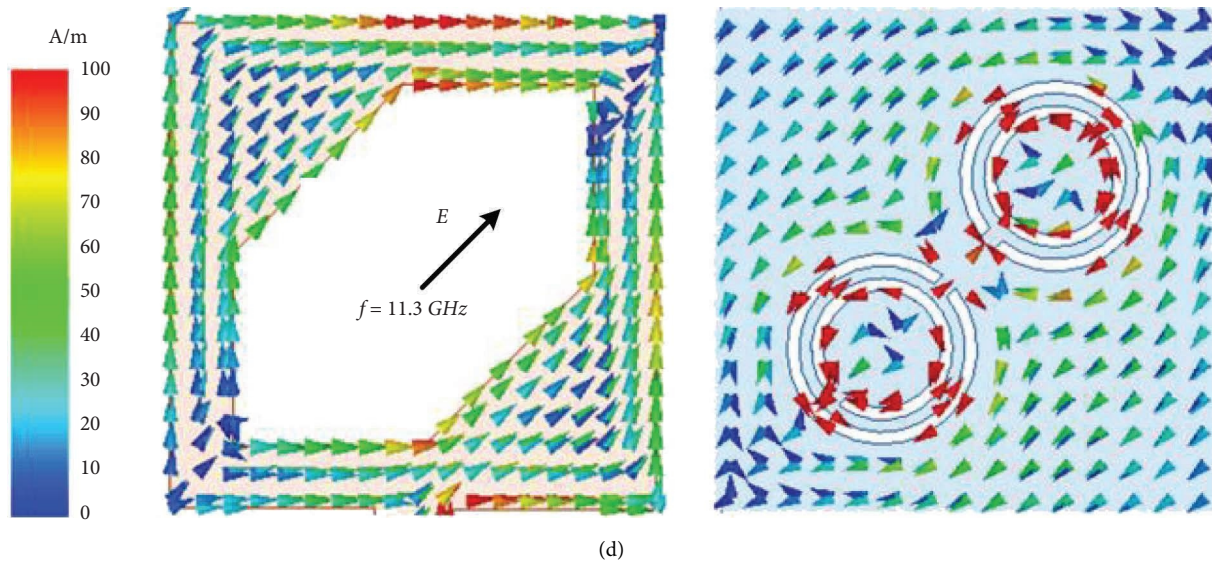


FIGURE 3: Current distributions on the top and bottom layers of the proposed antenna at resonant and notch frequencies: (a) 9.5 GHz, (b) 10.5 GHz, (c) 11 GHz, and (d) 11.3 GHz.

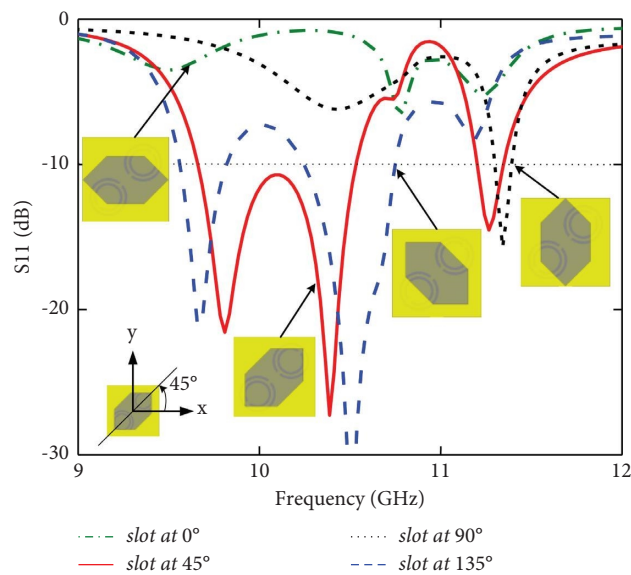


FIGURE 4: Simulated reflection coefficient of the antenna with different orientations of the slot.

4. Experimental Results

The proposed antenna was fabricated and measured to verify the simulation results. Figure 9 shows the measured reflection coefficient (S_{11}), which is consistent with the simulations, except for a slight downward frequency shifting at the highest resonance and notch band. This small frequency shift is of 0.1 GHz (about 0.90%) at both the highest operating frequency and the notch band, where the simulated center frequencies of the notch band and the highest

resonant band are 10.8 GHz and 11.4 GHz and the measured ones appear at 10.7 GHz and 11.3 GHz, respectively. This may be attributed to fabrication tolerances due to the relatively small CSRR dimensions. The measurement shows three operating bands of the antenna within the X-band. The center frequencies and -10 dB bandwidths of the operating bands are 9.5 GHz and 300 MHz, 10.5 GHz and 300 MHz, and 11.2 GHz and 297 MHz, respectively. The fabricated antenna also provides a notch band from 10.6 to 11.05 GHz with its maximum at 10.7 GHz.

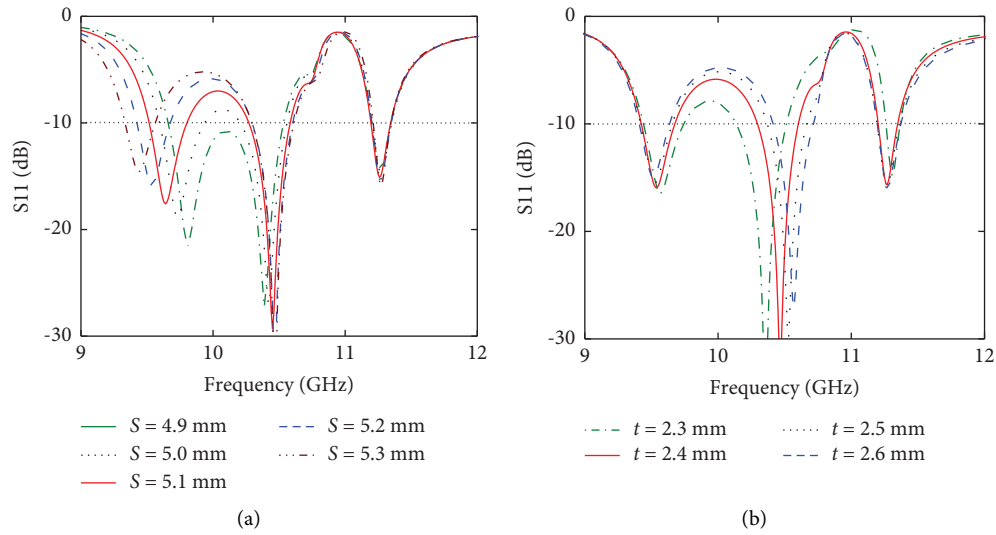


FIGURE 5: Reflection coefficient of the proposed antenna when tuning the slot dimensions by adjusting (a) S and (b) t .

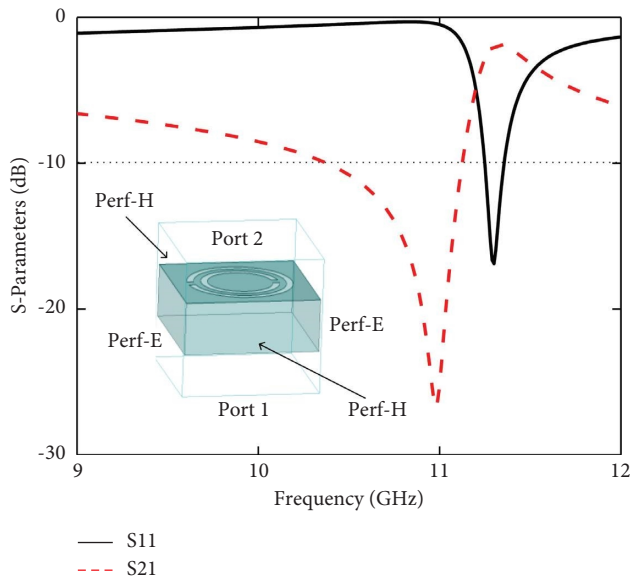


FIGURE 6: Simulated S-parameters of the CSRR unit-cell. Inset: boundary conditions of the unit-cell simulation.

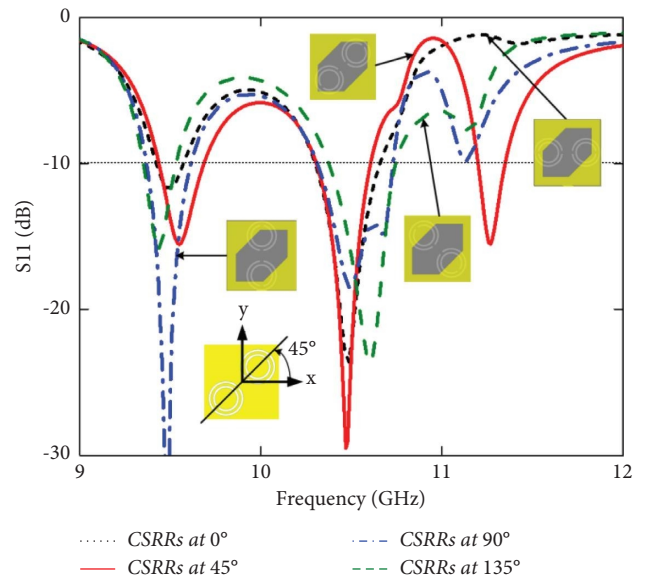


FIGURE 7: Simulated reflection coefficients of the antenna when rotating CSRRs.

The far-field measurement of the fabricated antenna is performed using a Satimo Starlab system (Figure 10), with the inset showing the top and bottom views of the fabricated antenna. As shown in Figures 11 and 12, the measured results show a good agreement with simulations. The lower measured gain and efficiency can be explained by the imperfection of fabrication and misalignment of the measurement setup due to the relatively small antenna prototype. As shown in Figure 11, the fabricated antenna shows a measured total efficiency and gain above 70% and 5

dBi within the operating frequency bands, respectively. Due to the losses of the feeding network and the measurement environment, the measured gains and efficiencies of the fabricated antenna are a little less than the simulated ones. Moreover, the efficiency and gain of the antenna degrade rapidly to around 10% and 0 dBi, respectively; at around 10.7 GHz, this observation means that a notched band is introduced here, as expected. Figure 12 shows the measured radiation patterns of the proposed antenna at its resonant frequencies in both E- and H-planes. It is worthy to note that

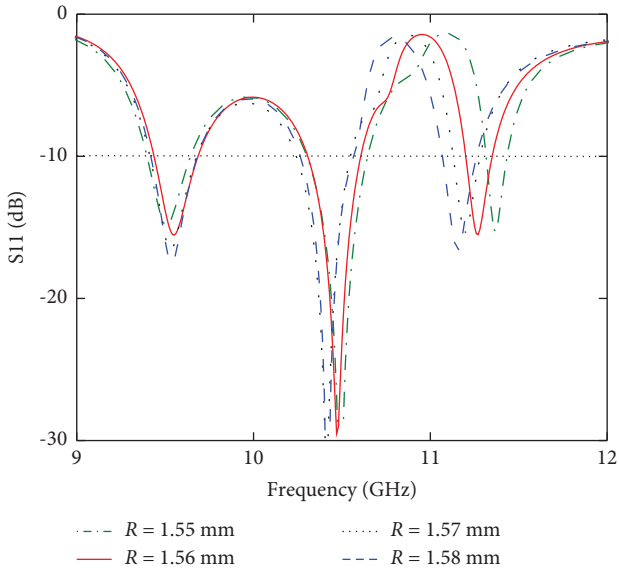


FIGURE 8: Simulated reflection coefficients of the antenna when adjusting R .

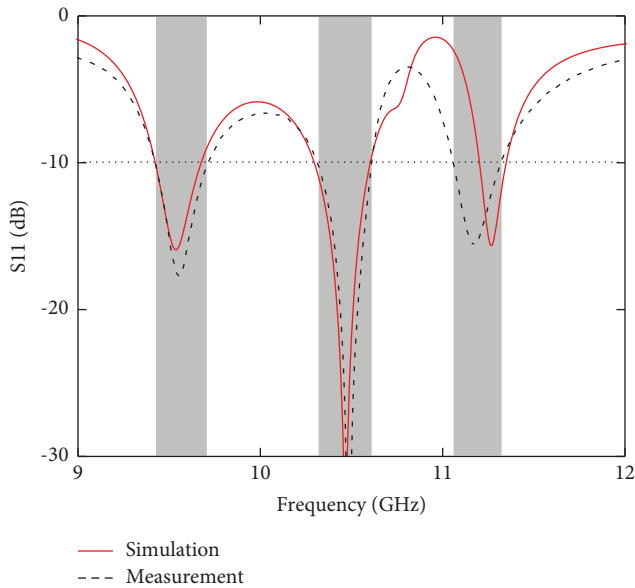


FIGURE 9: Simulated and measured reflection coefficient of the proposed antenna.

at 9.5 GHz, the E-plane is the plane spanned by the boresight z -axis and the horizontal axis that has been rotated by $\phi = -45^\circ$ (rotated around the z -axis looking towards the antenna), as shown in Figure 3. Meanwhile at 10.5 GHz and 11.3 GHz, the E-plane contains the z -axis and the horizontal axis rotated by $\phi = 45^\circ$. In general, the antenna shows a directional radiation pattern at three resonances at 9.5, 10.5, and 11.3 GHz with the main lobe of the antenna directed towards the $+z$ -direction. At 9.5 GHz and 10.5 GHz, the radiation patterns are similar to that of a conventional patch

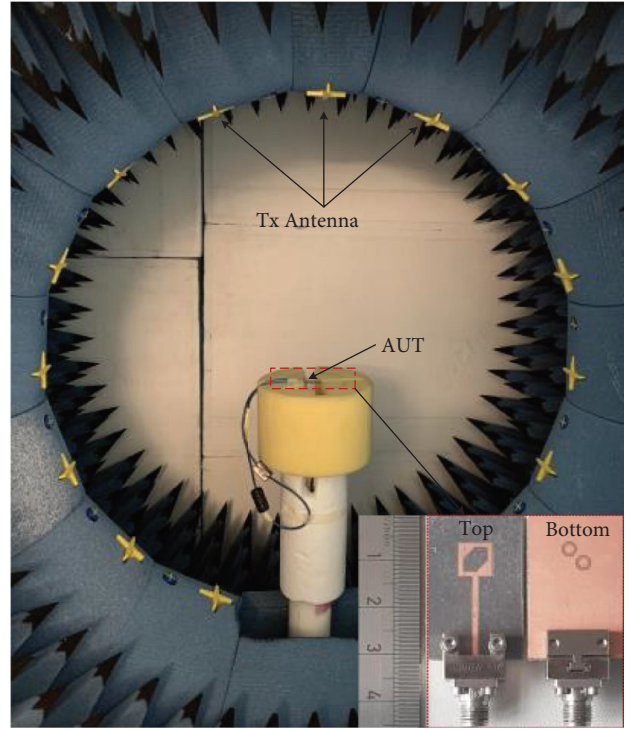


FIGURE 10: Measurement setup of the fabricated antenna in an anechoic chamber (inset photo shows the fabricated antenna).

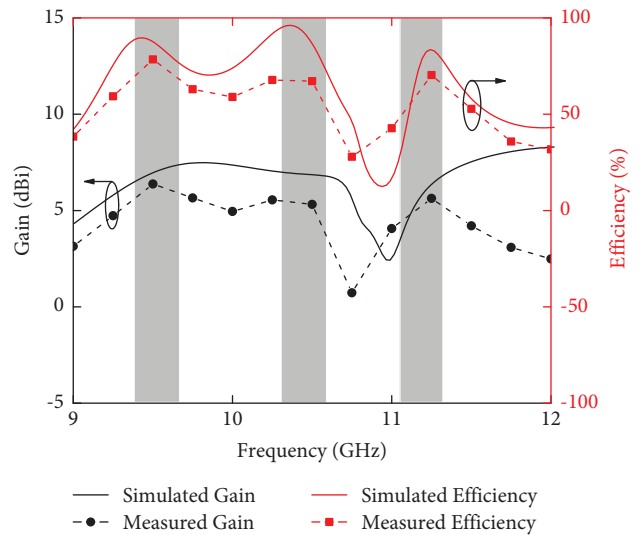


FIGURE 11: Simulated and measured peak gain and total efficiency versus the frequency of the proposed antenna.

antenna. However, at 11.3 GHz, the proposed antenna shows a larger back lobe due to resonance of the CSRR structures etched into the ground plane at this frequency, as mentioned above.

Table 2 compares the proposed antenna with other relevant compact planar multiband antennas reported in the literature. The proposed antenna exhibits the highest

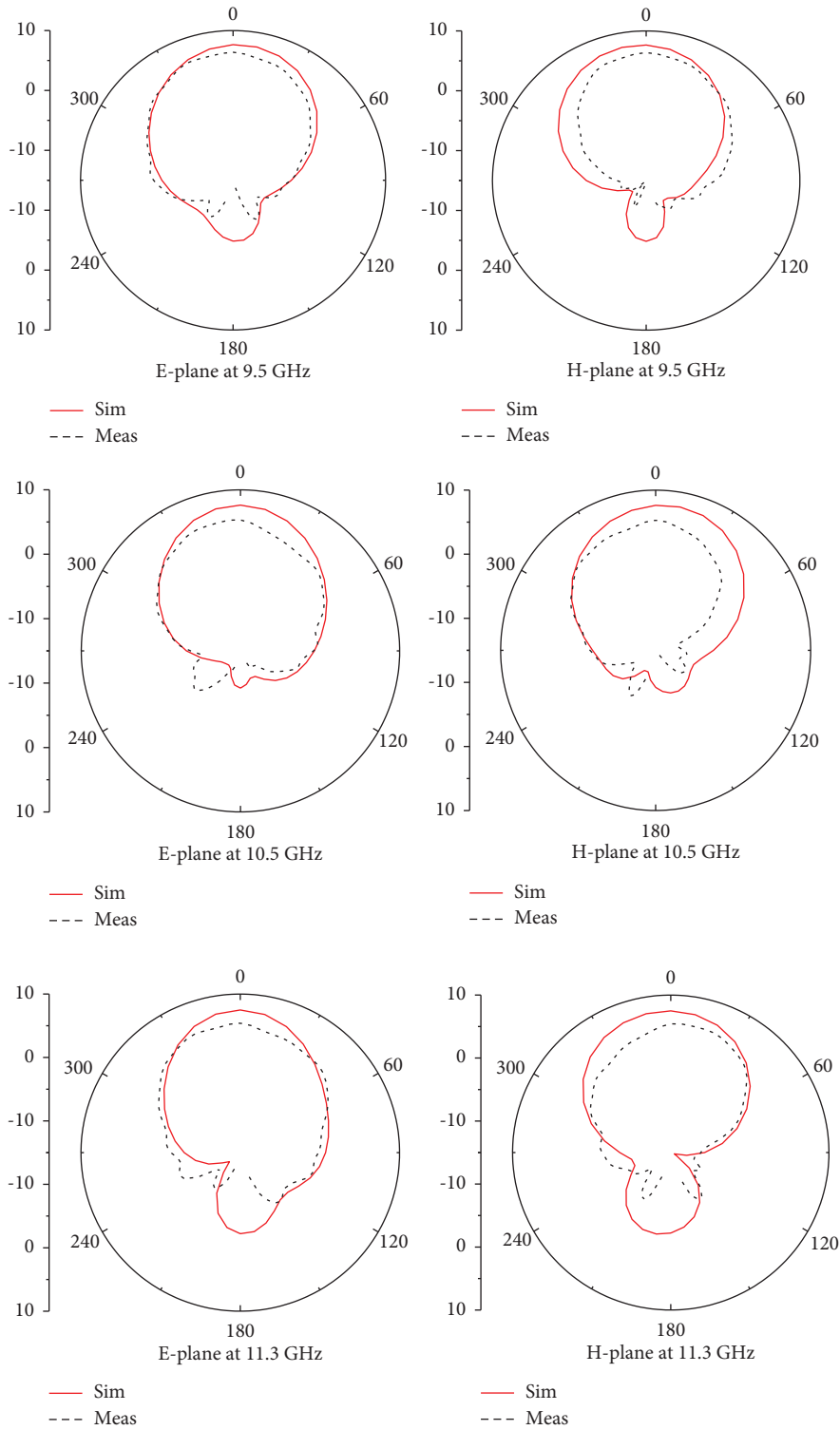


FIGURE 12: Simulated and measured radiation patterns at the three operating frequencies of the proposed antenna.

operating frequencies at the X-band with moderate gain levels. In addition to that, the proposed antenna is one of the simplest design with a single-layered substrate, which can be

easily fabricated using conventional PCB technology. On the other hand, the proposed antenna is the second one among the given works that show an independent frequency tuning

TABLE 2: Performance comparison between the proposed antenna with existing works.

References	Dimensions (L × W × h)	Operating frequency (GHz)	Bandwidths	Gain (dBi)	No. of layer	Freq. Tuning
[1]	$1.2\lambda_0 \times 0.42\lambda_0 \times 0.1\lambda_0$	3.5–3.75, 4.85–5.2, and 5.5–5.7	8.1, 8.0, and 7.9	6.9, 7.0, and 3.6	3	Dependent
[2]	$1.43\lambda_0 \times 1.17\lambda_0 \times 0.102\lambda_0$	1.59–1.68, 1.8–1.84, 1.93–1.98, 2.1–2.11, and 2.23–2.35	5.5, 2.0, 2.7, 1.5, and 5.3	9.2, 8.4, 7.6, 6.9, and 7.3	17	Dependent
[3]	$0.34\lambda_0 \times 0.65\lambda_0 \times 0.015\lambda_0$	2.28–2.57, 5.0–6.27, and 7.11–7.96	12.0, 22.5, and 11.3	1.5, 2.6, and 3.1	3	Dependent
[4]	$0.46\lambda_0 \times 0.72\lambda_0 \times 0.14\lambda_0$	2.84–3.39 and 4.5–4.83	17.6 and 7.1	5.9 and 6.2	5	Independent
[5]	$0.24\lambda_0 \times 0.13\lambda_0 \times 0.005\lambda_0$	0.865–0.88, 1.525–1.605, 1.79–1.868, and 2.085–2.125	1.7, 5.1, 4.2, and 1.9	1.29, 3.94, 1.15, and 0.89	3	Dependent
This work	$0.64\lambda_0 \times 0.99\lambda_0 \times 0.05\lambda_0$	9.4–9.7, 10.3–10.6, and 11.05–11.32	3.1, 2.9, and 2.4	6.3, 5.3, and 5.6	3	Independent

characteristic. Considering all these advantages, the proposed triband antenna is a practical candidate for applications in the X-band such as motion sensing or radar-activated obstruction lighting system for wind turbines.

5. Conclusions

This paper presented triband antennae with integrated notch-band characteristics while maintaining design simplicity. The proposed antenna is a patch loaded with a slot and two CSRR structures in the ground plane, allowing it to operate at three frequency bands and exhibit a band-notch behavior (at 10.7 GHz) within the X-band. Most importantly, the resonant frequencies of the antenna can be controlled independently by varying the dimensions of the slot and CSRR structures. The measurement results validated this antenna operating in three bands in the X-band including (with absolute and relative bandwidths) 9.4–9.7 GHz (300 MHz, 3.14%), 10.3–10.6 GHz (300 MHz, 2.86%), and 11.05–11.32 GHz (297 MHz, 2.66%) with an average gain and efficiency of 6.3 dBi, 78%; 5.3 dBi, 67%; and 5.6 dBi, 70%, respectively. From these results, the proposed antenna can be considered as a potential candidate for sensing and radar applications in the X-band. The proposed antenna has only one notch band, a multiband antenna with multiple notch bands will be more desirable. The CSRR (or SRR) structures with different dimensions should be combined in the future work to design a multiband antenna. Section 5 clearly explains the main findings and implications of the work, highlighting its importance and relevance.

Data Availability

The data used to support the findings of this study are included within the article.

Conflicts of Interest

The authors declare that they have no conflicts of interest.

Acknowledgments

The authors would like to thank Dr. Markus Berg and Mr. Jiangcheng Chen from the University of Oulu for supporting the antenna measurements. This study was funded by the Ministry of Education and Training of the Socialist Republic of Vietnam; Institut für Hochfrequenztechnik, Technische Universität Braunschweig, 38106 Braunschweig, Germany; Centre for Wireless Communications-Radio Technologies, University of Oulu, FI-90014 Oulu, Finland. Open Access funding enabled and organized by Projekt DEAL.

References

- [1] W. C. Mok, S. H. Wong, K. M. Luk, and K. F. Lee, "Single-layer single-patch dual-band and triple-band patch antennas," *IEEE Transactions on Antennas and Propagation*, vol. 61, no. 8, pp. 4341–4344, 2013.
- [2] J. Anguera, G. Font, C. Puente, C. Borja, and J. Soler, "Multifrequency microstrip patch antenna using multiple stacked elements," *IEEE Microwave and Wireless Components Letters*, vol. 13, no. 3, pp. 123–124, 2003.
- [3] R. Zhi, M. Han, J. Bai, W. Wu, and G. Liu, "Miniature multiband antenna for wlan and x-band satellite communication applications," *Progress In Electromagnetics Research Letters*, vol. 75, pp. 13–18, 2018.
- [4] K. Kandasamy, B. Majumder, J. Mukherjee, and K. P. Ray, "Dual-band circularly polarized split ring resonators loaded square slot antenna," *IEEE Transactions on Antennas and Propagation*, vol. 64, no. 8, pp. 3640–3645, 2016.
- [5] A. D. Boursianis, M. S. Papadopoulou, J. Pierezan et al., "Multiband patch antenna design using nature-inspired optimization method," *IEEE Open Journal of Antennas and Propagation*, vol. 2, pp. 151–162, 2021.
- [6] A. Boukarkar, X. Q. Lin, Y. Jiang, and Y. Q. Yu, "Miniaturized single-feed multiband patch antennas," *IEEE Transactions on Antennas and Propagation*, vol. 65, no. 2, pp. 850–854, 2017.
- [7] W. Ali, E. Hamad, M. Bassiuny, and M. Hamdallah, "Complementary split ring resonator based triple band microstrip antenna for wlan/wimax applications," *Radio Engineering*, vol. 26, no. 1, pp. 78–84, 2017.
- [8] N. Bayatmaku, P. Lotfi, M. Azarmanesh, and S. Soltani, "Design of simple multiband patch antenna for mobile communication applications using new e-shape fractal," *IEEE Antennas and Wireless Propagation Letters*, vol. 10, pp. 873–875, 2011.
- [9] M. Ojaroudi, S. Yazdanifard, N. Ojaroudi, and R. Sadeghzadeh, "Band-notched small square-ring antenna with a pair of t-shaped strips protruded inside the square ring for uwb applications," *IEEE Antennas and Wireless Propagation Letters*, vol. 10, pp. 227–230, 2011.
- [10] J. R. Kelly, P. S. Hall, and P. Gardner, "Band notched uwb antenna incorporating a microstrip open-loop resonator," *IEEE Transactions on Antennas and Propagation*, vol. 59, no. 8, pp. 3045–3048, 2011.
- [11] W.-S. Chen and K.-Y. Ku, "Band-rejected design of the printed open slot antenna for wlan/wimax operation," *IEEE Transactions on Antennas and Propagation*, vol. 56, no. 4, pp. 1163–1169, 2008.
- [12] W. Jiang and W. Che, "A novel uwb antenna with dual notched bands for wimax and wlan applications," *IEEE Antennas and Wireless Propagation Letters*, vol. 11, pp. 293–296, 2012.
- [13] O. P. Kumar, P. Kumar, and T. Ali, "A compact dual-band notched uwb antenna for wireless applications," *Micro-machines*, vol. 13, no. 1, p. 12, 2021.
- [14] A. Bhattacharya, B. Roy, S. K. Chowdhury, and A. K. Bhattacharjee, "Compact slotted UWB monopole antenna with tuneable band-notch characteristics," *Microwave and Optical Technology Letters*, vol. 59, no. 9, pp. 2358–2365, 2017.
- [15] A. De, B. Roy, A. Bhattacharya, and A. K. Bhattacharjee, "Investigations on a circular UWB antenna with Archimedean spiral slot for WLAN/Wi-MAX and satellite X-band filtering feature," *International Journal of Microwave and Wireless Technologies*, vol. 14, no. 6, pp. 781–789, 2022.
- [16] L. Peng and C.-L. Ruan, "Uwb band-notched monopole antenna design using electromagnetic band gap structures," *IEEE Transactions on Microwave Theory and Techniques*, vol. 59, no. 4, pp. 1074–1081, 2011.
- [17] A. Abbas, N. Hussain, J. Lee, S. G. Park, and N. Kim, "Triple rectangular notch uwb antenna using ebg and srr," *IEEE Access*, vol. 9, pp. 2508–2515, 2021.

- [18] P. K. Sharma and N. Gupta, "A cpw-fed circular srr-inspired flexible antenna using polydimethylsiloxane (pdms) substrate for wlan and wban applications," *IEEE Journal on Flexible Electronics*, vol. 1, no. 1, pp. 39–46, 2022.
- [19] Z. A. A. Hassain, M. M. Ali, and A. R. Azeez, "Single and dual band-notch uwb antenna using srr/csrr resonators," *Journal of Communications*, vol. 14, no. 6, pp. 504–510, 2019.
- [20] J. Y. Siddiqui, C. Saha, and Y. M. Antar, "Compact srr loaded uwb circular monopole antenna with frequency notch characteristics," *IEEE Transactions on Antennas and Propagation*, vol. 62, no. 8, pp. 4015–4020, 2014.
- [21] S. Kundu and S. K. Jana, "Leaf-shaped cpw-fed uwb antenna with triple notch bands for ground penetrating radar applications," *Microwave and Optical Technology Letters*, vol. 60, no. 4, pp. 930–936, 2018.
- [22] D. Phan, H. Phan, and T. Nguyen, "A miniaturization of microstrip antenna using negative permittivity metamaterial based on csrr loaded ground for wlan applications," *Journal of Science and Technology*, vol. 54, no. 6, pp. 689–697, 2016.
- [23] A. B. Numan and M. S. Sharawi, "Extraction of material parameters for metamaterials using a full-wave simulator [education column]," *IEEE Antennas and Propagation Magazine*, vol. 55, no. 5, pp. 202–211, Oct. 2013.
- [24] T. Koschny, P. Markos, D. Smith, and C. Soukoulis, "Resonant and antiresonant frequency dependence of the effective parameters of metamaterials," *Physical Review*, vol. 68, no. 6, Article ID 065602, 2003.
- [25] N. I. Landy, S. Sajuyigbe, J. J. Mock, D. R. Smith, and W. J. Padilla, "Perfect metamaterial absorber," *Physical Review Letters*, vol. 100, no. 20, Article ID 207402, 2008.